Full paper

Flexible self-charging supercapacitor based on graphene-Ag-3D graphene foam electrodes

Libu Manjakkal, Carlos García Núñez, Wenting Dang, Ravinder Dahiya*

Bendable Electronics and Sensing Technologies (BEST) Group, School of Engineering, University of Glasgow, G12 8QQ, UK

ABSTRACT

A flexible three-dimensional porous graphene foam-based supercapacitor (GFSC) is presented here for energy storage applications. With a novel layered structure of highly conductive electrodes (graphene-Ag conductive epoxy–graphene foam), forming an electrochemical double layer, the GFSC exhibits excellent electrochemical and supercapacitive performance. At a current density of 0.67 mA cm^{-2}, the GFSCs show excellent performance with areal capacitance (38 mF cm^{-2}) about three times higher than the values reported for flexible carbon-based SCs. The observed energy and power densities (3.4 μW h cm^{-2} and 0.27 mW cm^{-2} respectively) are better than the values reported for carbon-based SCs. Analyzed under static and dynamic bending conditions, the GFSCs are stable with up to 68% capacitance retention after 25000 charge–discharge cycles. The light-weight, cost-effective fabrication and no self-heating make the GFSCs a promising alternative to conventional source of energy in the broad power density ranging from few nW cm^{-2} to mW cm^{-2}. In this regard, GFSC was integrated with a flexible photovoltaic cell resulting in a flexible self-charging power pack. This pack was successfully utilized to power continuously a wearable CuO nanorod based chemi-resistive pH sensor.

1. Introduction

Smart energy systems, comprising of efficient harvesting, storage and energy management components are critical for portable electronic applications such as wearable systems [1], defence [2], transportation [3], fashion [4], etc. In particular, the advanced technologies that are expected to be used for healthcare monitoring, such as e-skin [5], smart-coatings, tattoos like sensing patches [6,7] involve a large number of sensing devices with a high energy budget demand. Likewise, other applications such as electric cars, aerial vehicles, robotics and artificial prosthesis, which have higher estimated energy budgets and on-board energy sources, will be benefited from the development of high-performance energy systems. Supercapacitors (SCs) have recently emerged as a promising route to address the energy needs in above applications [8–10].

To this end, the enhanced energy-conversion mechanisms through various harvesting technologies based on photovoltaics (PVs) [11,12], piezoelectrics [13] and triboelectrics [14], have also been extensively investigated. Towards addressing the flexibility/stretchability requirements of wearable systems [15,16], PV cells and triboelectric/piezo-electric nanogenerators [14], with suitable form factors have been investigated [17,18]. While significant advances have been made in energy harvesting field, there is also a need to develop a suitable technology to store the excess of energy. Conventional Li-ion based batteries (LiB) (< 500 W h kg^{-1}) are not suitable for portable/wearable systems because they are heavy, bulky and have poor performance. Further, the heat produced by commercially available batteries can damage the human skin [19] and thus limits their use in wearable systems [3,5,20]. For these reasons, SCs have emerged as a promising alternative to conventional Li-ion batteries [8–10]. SC have high energy density (in the range of mWh cm^{-2}) and power density (range of W cm^{-2}) (see Ragone's plot in Fig. S1 in Supplementary information), fast charging time (~ 1 min), and high life cycle ($> 10^6$ cycles). Moreover, SCs present attractive features such as high flexibility, no thermal breakdown and environmental-friendly active/passive materials. These features make SCs the excellent candidate for flexible and portable energy storing devices [21,22].

Based on the fundamental principle, SCs mainly work through approaches of electrochemical double layer capacitor (EDLC) [22,23] and pseudo-capacitor (PC) [23,24]. By combining the EDLC and PC concepts, a third category, namely hybrid battery type supercapacitor (HSC) [25] has also emerged recently. Compared to PCs and HSCs, EDLCs have more stable performance ($> 10^6$ cycles), higher flexibility and simpler fabrication procedures [22,23,26,27], which make EDLCs suitable for portable/wearable applications. In contrast to the LiB technology with high limitations in the energy storage capacity, the

Table 1
Comparison of the areal capacitance and corresponding energy and power densities of EDLCs based SCs.

Material	Electrolyte	Areal Capacitance	Energy density	Power density	Ref
3D-graphene/ graphite-paper (full cell)	PVA-H_2SO_4	9 mF cm^{-2} at 0.05 mA	1.24 µW h cm^{-2}	0.0245 mW cm^{-2}	[28]
Ultrathin Planar CVD Graphene film	H_3PO_4	0.394 mF cm^{-2}	2.8 nW h cm^{-2}	2 µW cm^{-2}	[37]
Wrinkled graphene film	H_2SO_4-PVA	5.33 µF cm^{-2}	0.27 nW h cm^{-2}	11.77 µW cm^{-2}	[38]
Graphene thin film	PVA/H_3PO_4	3.7 mF cm^{-2}	0.235 µW h cm^{-2}	0.106 mW cm^{-2}	[39]
Electrochemically activated rGO film	PVA/H_3PO_4	11.15 at 1 mA cm^{-2} 15.38 at 0.1 mA cm^{-2}	–	–	[40]
Onion-like carbon	Et_4NBF_4/propylene carbonate	1.7 at 1 V s^{-1}	1×10^{-2} W h cm^{-3}	1 kW cm^{-3}	[41]
Nitrogen-doped rGO (flexible)	PVA/H_3PO_4	3.4 at 20 µA cm^{-2}	3.0×10^{-4} W h cm^{-3}	0.2 W cm^{-3}	[43]
rGO/CNT	3 M KCl	6.1 at 0.01 V s^{-1}	0.7 mW h cm^{-3}	77 W cm^{-3}	[44]
rGO	PVA/H_2SO_4	0.95 at 0.43 mA cm^{-2}	…..	…..	[45]
Laser-induced Graphene	H_2SO_4/PVA	9 at 0.02 mA cm^{-2}			[46]
Graphene Foam based SC	H_3PO_4	38 mF cm^{-2} at 0.67 mA cm^{-2}	3.4 µW h cm^{-2}	0.27 mW cm^{-2}	This work

features of SCs have demonstrated great scalability, i.e. SCs are expected to power efficiently from low to high-power consumption devices. In this regard, the main characteristics of SC subjected to intensive investigations are the areal capacitance (C_A), energy density (E_A) and power density (P_A). For example, 3D-graphene/graphite-paper based SCs showing record values of C_A (9 mF cm^{-2}), E_A(1.24 µW h cm^{-2}), and P_A(25 µW cm^{-2}) [28], it is still an energy storage technology limited to power flexible micro-/nano-devices with power consumption in the range of mW cm^{-2} and nW cm^{-2} (Table 1). Here, we further enhanced the capability of carbon materials by demonstrating promising results with EDLCs based on 3D graphene foam (GF) as electrodes. We take the advantage of the porosity in GF to increase the effective surface area of the electrode, and therefore, to obtain a faster and efficient electron transport through rapid the ion exchange mechanism [29,30]. A few GF-based SCs (GFSCs) reported in literature have used composite of GF with metal oxides (MnO_2, Co_3O_4) [29,31] or polymers (polypyrrole, PANi) as electrodes [32,33]. Generally, these electrodes present good electrochemical performance, but they have a low electrochemical stability under long-lasting charge-discharge cycles. This is either because of Faradaic redox reactions or the mechanical degradation observed in metal oxide. In the case of polymer-based electrodes, SCs are relatively stable, but their low electrical conductivity still remains a bottleneck as it hinders the electron transfer through the active material (e.g. GF with polyurethane (PU)) [34].

In this work, we present for the first time an EDLC SC based on free standing GF as electrode, with highly improves electron transfer from electrode to the active material. The new SC electrode structure reported here consists of a highly conductive graphene sheet (GS) as a current collector and GF as active material, both bonded with Ag conductive epoxy. The resulting SCs based on GS-Ag-GF layered electrodes were characterized by cyclic voltammetry (CV), electrochemical impedance spectroscopy (EIS) analysis and galvanostatic charging discharging (GCD) method. In addition, the performance of developed GFSCs is compared with state-of-the-art SCs (Table 1). GFSCs were also characterized under static and dynamic bending conditions as well as tested for 25000 charging/discharging cycles. To demonstrate the applicability in wearable systems, the GFSCs were integrated on a flexible PV cell and a flexible fully self-charging power pack (FSPP) was obtained. The observed capacitance (38 mF cm^{-2}), energy and power densities (3.4 µW h cm^{-2} and 0.27 mW cm^{-2} respectively) are beneficial for low power wearable sensors. New technologies are rapidly evolving towards the development of self-powered systems with energy harvesters and storage devices on non-conventional flexible substrates. In this regard, triboelectric generator, piezoelectric generator and solar cells are considered as promising candidates [35]. However, the critical challenge is the variable power generation for energy harvesting such as solar cells where sunlight may not available all the time. In this regard, a flexible energy storage device is necessary. A comparison between recently reported self-powered systems for wearable applications

is given in Table S1 in the Supplementary information. The FSPP was successfully used as a direct current (DC) source for the continuous powering of a flexible chemi-resistive pH sensor [36], to demonstrate the promise the presented SCs hold for fully self-powered flexible sensors for health monitoring applications.

2. Experimental section

2.1. Fabrication of electrodes

The fabrication steps of GFSC electrodes are described in Fig. 1. Firstly, PU has been drop-casted on top of a 3 × 1.5 cm^2 flexible polyethylene glycol terephthalate (PET) substrate (Fig. 1(a)). Thereafter, multi-layered GS consisting of 300 layers of stacked GS (from Graphene Super Market, USA) was adhered on the top of the PU (Fig. 1(b)), having the role of charge collector. Resulting sample was annealed at 80 °C for 2 h. After bonding to GS, Ag conductive epoxy (from RS components, 186–3600) was printed on the top of GS, partially covering an area of 3 cm^2 (Fig. 1(c)). Then, 3 cm^2 GF (from Graphene Super Market, USA) has been deposited atop the area covered by the Ag epoxy and cured at room temperature for 1 h to ensure the proper bonding of GS and GF (Fig. 1(d)). The Ag conductive epoxy provides excellent adhesion between GS and GF. The high conductivity of the epoxy reduces the contact resistance between the electrodes as shown later. As connection pad, a Cu strip was connected to external terminals of the SC (Fig. 1(e)), using a protective PU layer to ensure the impermeable encapsulation of those areas that will be in contact with the electrolyte. Thereafter, the electrolyte (H_3PO_4) were dropped on top of the GF area, followed by the deposition of a polyester/cellulose blend separator (Techni Cloth, TX 612) on top of the wet area (Fig. 1(f)). The separator is meant to act as an ion permeable membrane and absorbent electrolyte for keeping wettability. The complete fabrication of the SC comprises the fabrication of two electrodes (Fig. 1(a)-(e)), and finally, their stacking as schematically illustrated in Fig. 1(g). To protect the GFSC from electrolyte leakage, the device was packed and encapsulated by using Kapton tape and then by polymer film.

2.2. Fabrication of chemi-resistive pH sensor

CuO nanostructured material was prepared by hydrothermal synthesis method and the sensitive electrode was fabricated by screen-printing method on a flexible PET substrate. A chemi-resistive CuO nano-rod based flexible pH sensor on PET substrate was fabricated by screen-printing method, as thoroughly described elsewhere [36].

2.3. Characterization of GFSC electrodes

Morphological characterization of as-fabricated GF electrodes was carried out by means of scanning electron microscope (SEM, SU8240 BRUKER, at 15 kV and WD of 8 mm). The SEM images were post
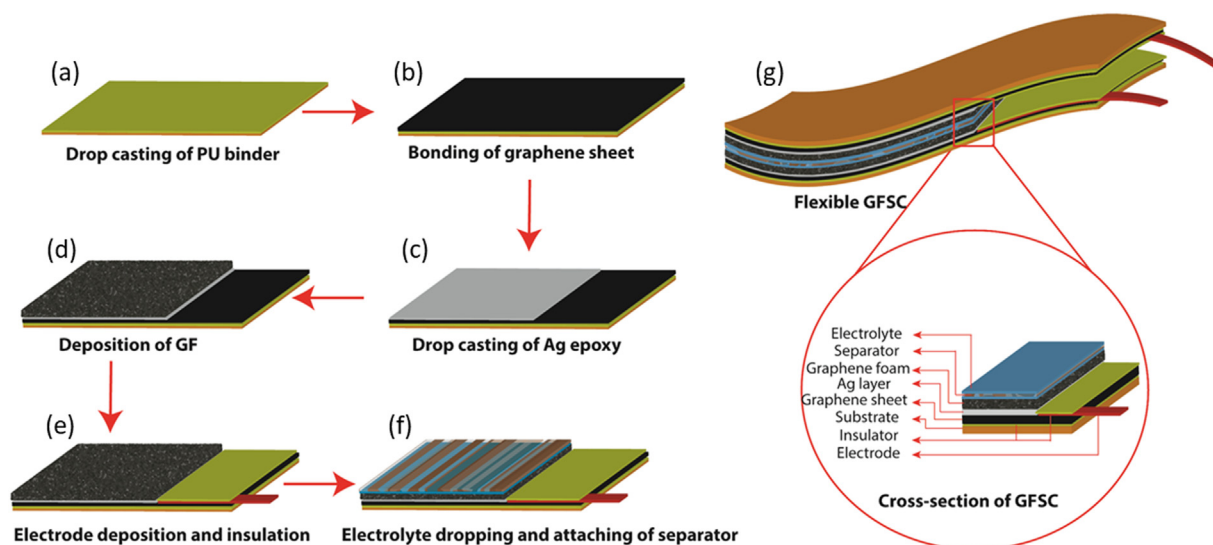
Fig. 1. 3D schematic illustration of the steps used to fabricate GFSC electrodes, comprising (a) drop-casting of PU binder on flexible PET, (b) deposition and bonding of GS atop PU layer, (c) printing of Ag layer on top of GS (d) deposition and bonding of GF on the area covered by the Ag layer, (e) deposition of Cu stripes and GS, (f) dropping of the electrolyte on a separator placed on top of the GF area and (g) stacking of two electrodes forming the GFSC full cell.

processed in ImageJ software (binary conversion and automated threshold), to define the pores boundaries and to calculate parameters such as pore size, and surface density. In addition to this, Brunauer-Emmett-Teller (BET) method (Quantachrome Evo, molecular cross section of the adsorbate molecule 16.2 Å^2 for N_2 at 77.3 K) was used for the surface area analysis of the materials by using adsorption data. The electrochemical and capacitive performance of the GFSC was analyzed by CV, EIS and GCD methods in a two electrodes system (Metrohm Autolab, PGSTAT302N). The CV analysis of the GFSC electrode was carried out at scan rates ranged between 5 and 200 mV s^{-1} in a potential range ranging between −1 and 1 V. The EIS analysis of GFSC was carried out by applying an alternating-current (AC) signal in the frequency range of 1–1 MHz and using a potential amplitude of 10 mV. The value of C_A, E_A and P_A of the GFSC were obtained through GCD measurements at various applied currents (I). The expression used to calculate these factors is presented in the Supplementary information. The response of GFSCs was characterized under static and dynamic bending conditions. On one hand, the static characterization of GFSCs performance was carried out by conformably wrapping the GFSC atop the surface of a 3D-printed semi-cylindrical piece (printed in a CubePro Trio 3D printer) with radius of 10 and 20 mm. On the other hand, the dynamic characterization was carried out by attaching GFSCs to two linear stages (from Micronix USA). Both stages were synchronized through LabVIEW's software, allowing to control their speed, acceleration and location over time, as well as, to move them along opposite directions. In this scenario, CGSCs were periodically bent at a speed of 0.5 mm/s.

2.4. Fabrication of flexible self-charging power pack (FSPP)

For the fabrication of the FSPP, three flexible GFSC modules (connected in series) was connected to an amorphous silicon (a-Si) flexible photovoltaic (PV) cell (from Sanyo, AT7665A 664-6841), placing the GFSC underneath the PV cell. The connection between the GFSC and PV cell was carried out through an evaluation board SPV1050 ULP (from STMicroelectronics) to optimize both the performance of the energy harvested by the PV cell and charging of the GFSC. The characterization of the FSPP was carried out under above dynamic cyclic bending conditions and exposing the surface of the PV cell to the white light emitted by a 250 W halogen lamp (from Philips, 261-2469) and located at 10 cm far from the PV cell surface.

2.5. FSPP as a future energy source for wearable pH sensors

As a preliminary investigation, the variation of resistance of pH sensitive electrode in pH test solutions were tested. The value of pH of solution is varied by adding diluted HCl or KOH into the solution under stirring. The experimental setup is shown in Fig. S2 in Supplementary information.

3. Results and discussion

3.1. Morphological properties of GF and GS

The morphological characterization of GF (Fig. 2(a)-(d)) and GS (Fig. 2(e)) has been carried out by SEM. The SEM image shows that the surface morphology of GF (Fig. 2(a)-(d)) has higher porosity than GS (Fig. 2(e)). Further, the GF has a 3D structure which mainly consists of carbon micro-structured flakes (Fig. 2(a)-(d)) with a random distribution of pores of average size of 50 nm^2 (Fig. 2(f)). In contrast, the GS presents a smooth surface with less defined grain boundaries, and therefore, lower roughness than GF (Fig. 2(e)). The porous structure and the rough surface of the GF are beneficial in terms of enhanced ion exchange in electrochemical reactions and thus contribute to enhance the electrochemical and capacitive performance of the SC as will be shown later. Initially, the pore size distribution of the electrodes has been analyzed post-processed SEM images with ImageJ as explained in Fig. S3 (Supplementary information). The surface area of the electrode influences the electrode-electrolyte interactions and energy storage [23,26]. The specific surface area of the electrode was measured by BET surface area analysis and is found to be 618 m^2/g. The N_2 adsorption and desorption curves of electrode for analysing the specific surface area of the samples is shown in Fig. S4. The adsorption and desorption isotherms using BET method are described in supplementary.

The thickness of electrode layers such as GF (~ 550 µm) and GS with epoxy (~ 15 µm) was obtained from cross-sectional SEM image as shown in Fig. S5 in supplementary. The contact angle measurement confirm that the 3D network foam-like structure reduces the hydrophobicity of GF with electrolyte, as compared to GS. The optical microscopic images of GS and GF, with and without contact of electrolyte, are shown in Fig. S6 in Supplementary information. Fig. S6a and S6b represent the film surface without electrolyte. The electrolyte is not spreading on the top of GS which is kept as a bubble on the top
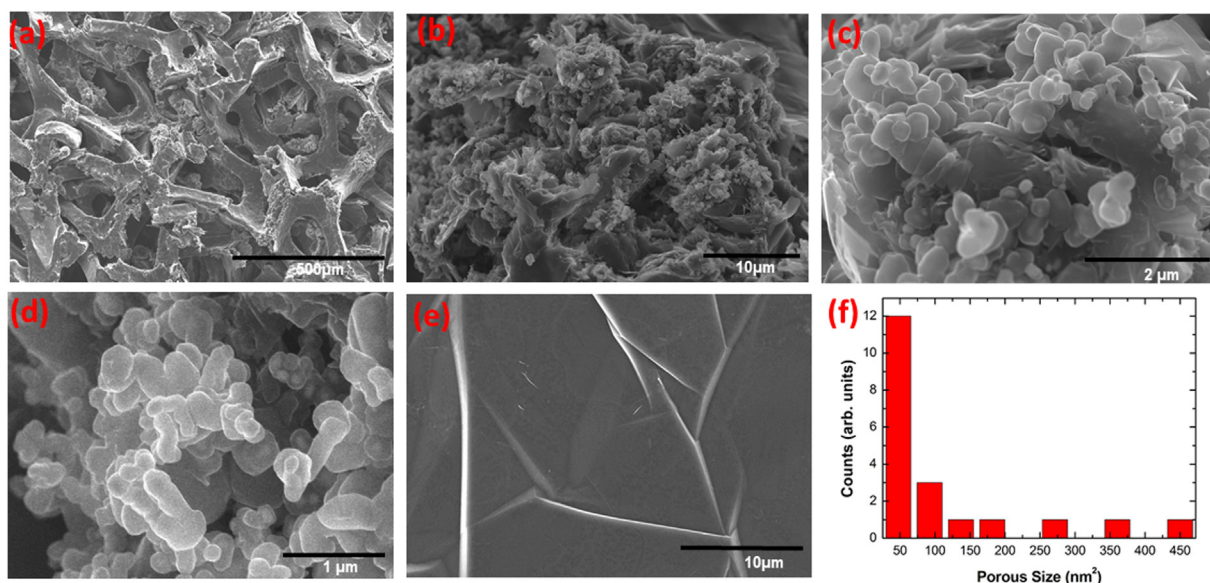
Fig. 2. SEM image of (a-d) GF and (e) GS at different magnification and (f) porosity of GF obtained from (d).

presented in Fig S6c. The observed contact angle for GS is around 70° (Fig. S7 in supplementary) and hence it shows hydrophobic nature while reacting with electrolyte. However, due to the porous 3D networks GF have a very good interaction with electrolytes as shown in Fig. S6d. The observed contact angle for the GF with electrolyte is almost 0° as shown in Fig. S7. The hydrophilic nature of GF enhances the electrochemical performance for energy storage by increasing the ionic exchange at electrode-electrolyte interface.

3.2. Electro-chemical properties of GFSC electrodes

The electro-chemical and electro-capacitive performance of GFSC electrodes have been investigated in the two-electrode system using H_3PO_4 as electrolyte. According to the general mechanism governing EDLC based SCs [23,37,38], positive (H^+) and negative (PO_4^{3-}, HPO_4^{2-} and $H_2PO_4^{4-}$) [39] ions from H_3PO_4 electrolyte are absorbed on the cathode and anode electrodes, respectively, during the charging step (Fig. 3(a)). The absorption of electrolyte positive and negative ions into SC electrodes by electrostatically or non-Faradaic reactions results in electrical double layer (*edl*). In GFSC electrodes, the *edl* occurs along the high surface area of the porous GF layer. The high surface area of porous GF and less hydrophobicity (shown in Fig. 2(f) and 2(i)) enhance the ion absorption (Fig. 3(a)) on the electrode surface and improve the charge storing capacity. During discharging, ions desorb from electrode surface and move to the electrolyte due to the absence of net electrical force. The good wettability of the H_3PO_4 electrolyte by using cellulose separator will facilitate the mobility of ions during both ion absorption and desorption mechanism into the pores of the GF electrodes. This will further enhance the capacitive performance of the proposed device and is evaluated in following section.

The CV and EIS analysis of the device were carried out to demonstrate above mechanisms and to study the electrochemical properties of GFSC electrode (Fig. 3). CV curves of a GFSC cell (Fig. 1(g)), measured at scan rates ranged between 5 and 200 mV s^{-1} are presented in Fig. 3b and Fig. S7 in Supplementary information. From these figures, it can be observed that CV presents a cyclic shape independently on the scan rate. However, the shape of the CV is strongly influenced by the scan rate, especially in the range of 5–50 mV s^{-1}, where the slope of the CV curve and maximum current levels exhibit smaller value than those obtained at higher scan rates in the range of 50–200 mV s^{-1} (the extended CV analysis shown in Fig. S8 in Supplementary). This result is in good agreement with the electrical current measured at 1 V as a

function of the scan rate (Fig. 3(c)), where the resulting current density increases with the scan rate. Above results are important to understand the behavior of a GFSC as energy storing device, directly varying properties such as acquired current density, operating voltages, etc. In particular, the increase of the maximum current levels up to 7.4 mA (0.5 < V < 1 V) obtained at a high scanning rates of 200 mV s^{-1} (Fig. 3b and Fig. 3c), would indicate a predominant diffusion mechanism governing the reaction of ions from the electrolyte to the GFSC electrode surface in addition to the general absorption mechanism. Moreover, the use of low scanning rates (5–20 mV s^{-1}) allows the observation of a redox peak at around 0.2 V with a maximum current of 6.3 mA (Fig. S8 in supplementary), which is due to the reaction at the interface between Ag and GF layers in addition to non-Faradaic reaction between the GFSC and electrolyte. This result demonstrates that the conductive Ag layer for bonding also contributes to the electrochemical reaction of fabricated GFSCs at low scanning rate.

EIS analysis has been carried out to further evaluate properties of GFSC electrodes, including ion exchange, charge transport and capacitive performance at electrode/electrolyte interface (Fig. 3(d)-(f)). Nyquist's plot presented in Fig. 3(d), shows a linear trend at lower frequencies (1 Hz–10 mHz), i.e. 40 < Z_{real} < 85 Ω, and a slope of 46°, reflecting the ideal capacitive nature of GFSC electrodes, and confirming the diffusion mechanism of ions through the electrode surface mainly favoured by the porosity of the GF structure (Fig. 2(d)). In this particular frequency range, the variation of resistance was observed between 25 and 85 Ω, which are extremely low values for ionic exchange and reveal a high and rapid ion interaction of GF active material with the electrolyte. This result partially explains the origin of the significant enhancement obtained in the electrochemical performance of the fabricated GFSCs. In the high frequencies region the resistance is below < 25 Ω and an inflection point is observed at ∼ 3 Ω in the Nyquist's plot (Fig. 3d). The concave downwards trend observed below 3 Ω (inset of Fig. 3(d)) is the characteristic curve of a charge-transfer process whose resistance is defined as charge transfer resistance (R_{ct}). The value of R_{ct} can be calculated from the radius of a circle fitting the concave downwards trend observed in Fig. 3(d). The calculations reveal a low R_{ct} (< 1 Ω), which is influenced by the Ag layer. The lower value of R_{ct} reveals that the contact resistance between the Ag conductive epoxy and GS is very low and is beneficial for the energy storage application. The non-zero intersection at high frequencies is due to the solution resistance (R_s) and one additional ohmic resistance from the active electrode material. R_s is estimated to be around 2.3 Ω (inset of
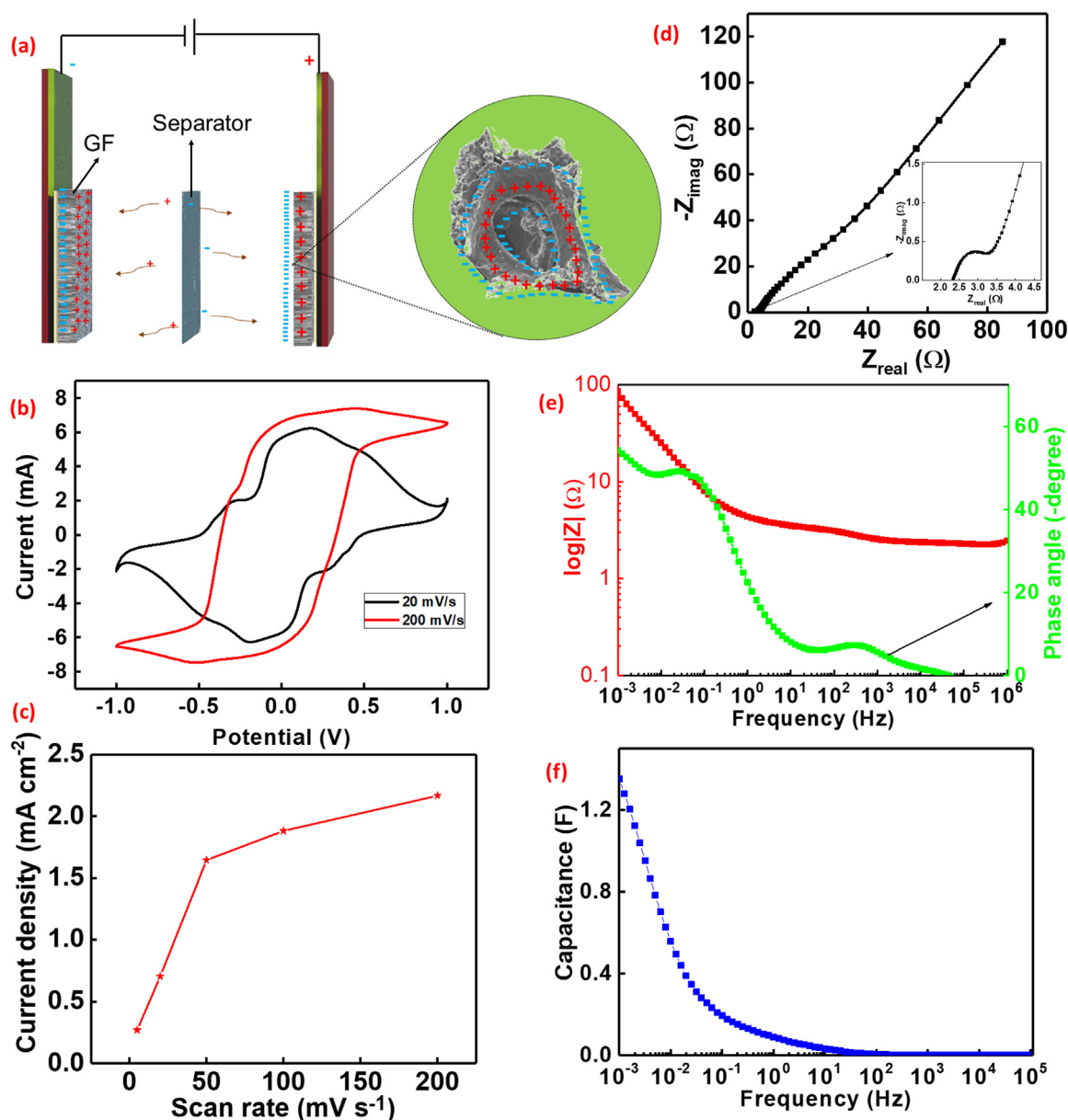
Fig. 3. (a) 3D schematic illustration of the electrochemical reaction observed at the surface of the GF electrode. (b) CV curve for scan rates of 20 and 200 mV s^{-1}. (c) Current density measured between electrodes vs. scan rate. (d) Nyquist plot (inset: high frequency range). (e) Bode impedance and phase angle plots. (f) Capacitance of GFSC vs. frequency.

Fig. 3(d)), reflecting the high conductivity of GFSC electrodes and low contact resistance between the electrode and electrolyte, which attribute to the excellent electrochemical/capacitive performance.

The Bode's plot obtained from EIS analysis (Fig. 3(e)) clearly shows the capacitive performance of the device. Due to ion diffusion, the Bode's impedance shows a linear decrease as the frequency increases from 1 to 10 mHz. The Bode impedance is almost constant in the high frequency range (10^4–10^6 Hz) because of the charge transfer effect and R_s. Hence, the solution and material resistance mainly define the device performance. Similarly, the Bode's angle reveals that at low frequencies, the phase angle reaches a maximum value of 55°, suggesting the capacitive nature of electrode. In this regard, the EIS analysis indicates that the electrolytes are easily accessible to the electrodes of GFSC and shows a maximum specific capacitance. The device has a specific capacitance of 1.3 F at 1 MHz (Fig. 3(f)). Therefore, EIS investigations confirm that the layered GS-Ag-GF electrode could be used for electrochemical SC applications.

To check the capacitance performance of the GFSC electrodes, GCD measurements were carried out under different current densities. By charging the GFSC full cell using 3 and 5 mA, we have observed that the maximum operating potential, i.e. saturation voltage, is 1.1 and 1.15 V, respectively (see Fig. S9 in Supplementary). For the sake of device protection, GCD measurements in this work were carried out limiting the maximum potential up to 0.8 V, which means, we switch SC to discharging mode right after the potential reaches 0.8 V (Fig. 4(a)). Ideally, graphene based SCs exhibit a triangular GCD curves due to non-Faradaic electrochemical reaction [40,41]. However, our GFSCs show a slight deviation from a straight line during the discharging step which can be explained due to the influence of conducting Ag epoxy. This result demonstrates the capacitive behavior of the device, which is a key feature for SC performance. Moreover, these results further confirm the electrochemical CV and EIS analysis and are in good agreement with reported GCD results with Ag incorporated electrodes [42]. In contrast to GFSC reported in the literature based on GF electrodes with
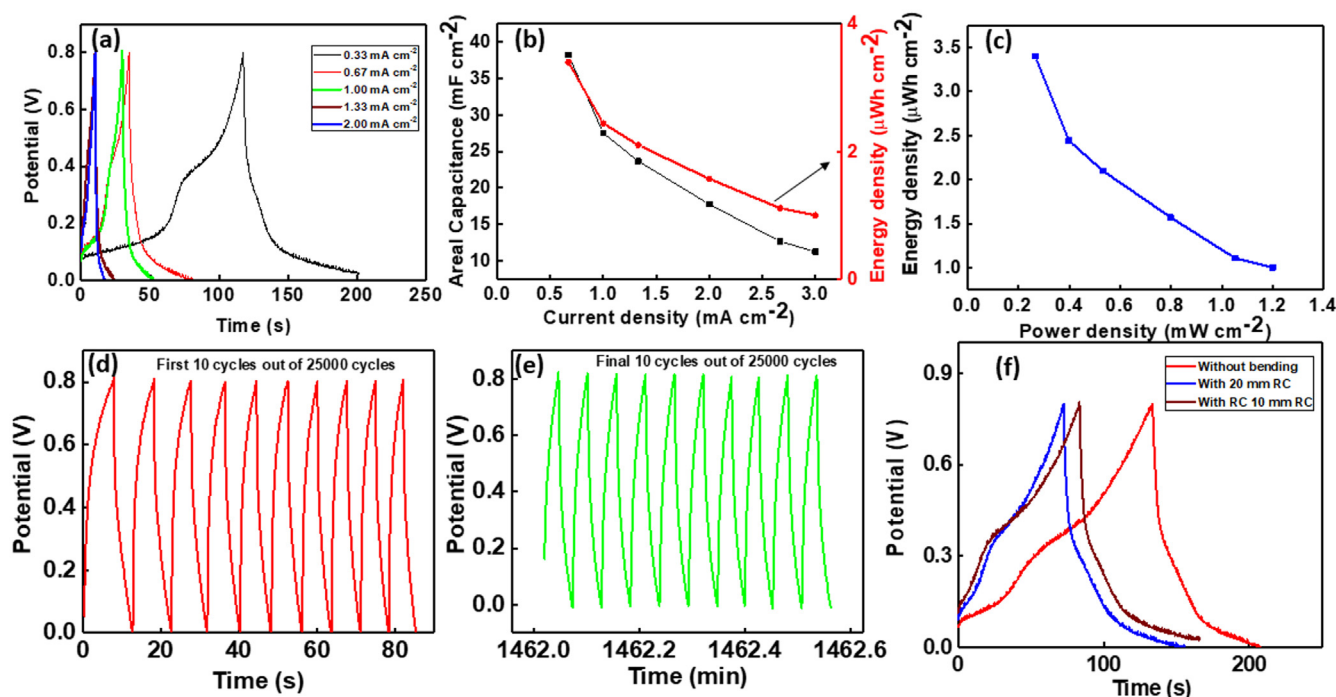
Fig. 4. (a) GCD curve of GFSC at different current densities. (b) Variation of C_A and E_A vs. current density. (c) Ragone plot of GFSC. (d) Initial and (e) final 10 cycles out of 25000 cycles of charging/discharging measurements. (f) GCD curve of GFSC measured different bending conditions.

Table 2
Comparison of GFSC performance measured in flat and bent conditions.

GFSC	Discharge Time (s)	Areal Capacitance (mF cm^{-2})	Energy density (µW h cm^{-2})	Power density (mW cm^{-2})
Without bending	84.8	35.75	3.1	0.13
20 mm radius of curvature	83.7	34.87	3.1	0.13
10 mm radius of curvature	82.6	34.41	3.0	0.13

polydimethylsiloxane or polyurethane, our electrode is based on free-standing GF, which enhances the conductivity and electrochemical performance of the GFSC electrode [34]. The C_A and E_A of the GFSC measured at current densities ranged between 0.33 and 3 mA cm^{-2} as shown in Fig. 4(b). The results show that both C_A and E_A decrease with current energy, exhibiting maximum values up to 38.25 mF cm^{-2} and 3.4 µW h cm^{-2}, respectively, for current densities of 0.67 mA cm^{-2}. The corresponding volumetric capacitance (C_V = 338 mF cm^{-3}) and energy density (E_V = 30 µW h cm^{-3}) of GFSC for the current density 0.67 mA cm^{-2} were measured by using expression (4) to (6) in Supplementary information. As compared to graphene based SCs, the observed areal capacitance of GFSC is 2–3 times higher (Table 1). There are various factors that can contribute for the C_A enhancement, comprising: 1) layer-by-layer structure of GS-Ag-GF electrode, 2) influence of Ag conductive paste on ion exchange mechanism, and 3) high conductive free-standing porous GF, facilitating the access of ions towards the *edl* structure. These factors also attribute to the SC performance in terms of energy and power density of the device. The GFSC exhibits an increase of the power density as the current density increases. The power density of GFSC is 0.27 mW cm^{-2} and 0.799 mW cm^{-2} at a current density of 0.67 mA cm^{-2} and 2 mA cm^{-2} respectively. The energy and power densities of 1.57 µW cm^{-2} (Fig. 4(b)) and 0.799 mW cm^{-2} are found at high current density of 2 mA cm^{-2} and they are shown in Ragone's plot in Fig. 4(c). In this regard, the observed value of areal energy and power densities show that the fabricated SCs have performance comparable to most SCs based on 1D graphene structures. For example, 0.27 nW h cm^{-2} at 11.77 µW cm^{-2} for wrinkled graphene films [38], and 1.24 µW h cm^{-2} at 25 µW cm^{-2} for 3D-graphene/graphite-paper [28]. Further comparison of the developed SC

with reported graphene based SCs is shown in the Ragone's plot in Fig. S1 in Supplementary and Table 1.

The stability of GFSCs was studied through 25000 charging-discharging cycles at 3 mA charging current. The initial 10 and final 10 cycles are shown in Fig. 4(d) and (e) to estimate the influence on SC after thousands of periodic charging/discharging cycles. From this comparison, it can be concluded that the fabricated GFSCs have excellent stability after 25k cycles and exhibit an extraordinary capacitive retention of about 68%. To validate our GFSC as an energy source for wearable applications, their performance was also analyzed under different static and dynamic bending conditions (Table 2). In static bending conditions, the GFSC was conformally attached to 3D printed cylindrical pieces with the radii 10 and 20 mm (inset of Fig. 5). The GCD characteristics measured under flat and bent conditions (using a charging current of 1 mA) are shown in Fig. 4(f). Results depict a significant influence from bending on SC charging time, but negligible influence on their discharging time.

To demonstrate the applicability of our GFSCs for self-powered wearable systems, we have also developed a FSPP by combining a GFSC with a flexible a-Si PV cell and flexible pH sensor. A 3D scheme of FSPP is shown in Fig. 5(b). Initially we tested the performance of charging discharging of GFSC by using flexible solar cell (image of hybrid is shown in Fig. S10 in Supplementary). The characteristics of the resulting solar cell with GFSC have been evaluated under different light illuminations, i.e. 0.5 sun and 1 sun (Fig. 5(c), with equivalent circuit in the inset), which can be considered as representative conditions observed during a cloudy and sunny day, respectively. From this analysis, we have obtained GFSC potentials of 0.27 and 0.87 V at 0.5 and 1 sun, respectively. The observed charging- discharging times and potential
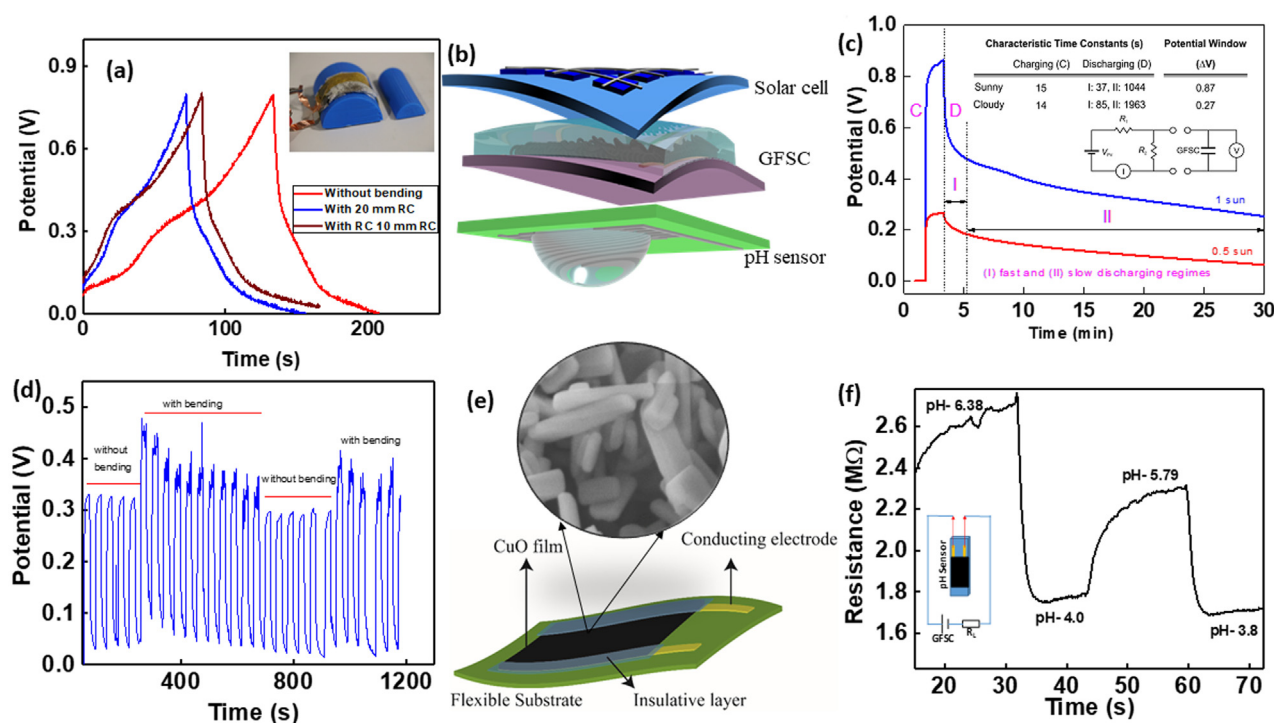
Fig. 5. (a) GCD curve of flat and bent GFSC under bending radius of 10 mm and 20 mm. (b) 3D schema of FSPP (flexible PV cell, GFSC and pH sensor) (c) charging/ discharging of GFSC by using flexible PV cell exposed to different light intensities (d) performance of GFSC and PV cell under dynamic bending conditions (e) Schematic of chemi-resistive pH sensor with an image of nanostructured CuO (f) chemi-resistive based pH sensor performance using GFSC as a voltage source.

with the light intensity are shown as Table in the inset of Fig. 5(c). It was found that at high potential the device discharge faster (37 s for 1 sun) than at low potential, where the discharging time was very slow (1044 s for 1 sun). Thus, the FSPP is suitable for low operating potential in wearable devices. FSPP has also been characterized under dynamic bending conditions (Fig. 5(d)) with bending at a speed of 0.5 mm/s. A minor shift in the potential window (~ 0.08 V) with and without bending was observed. The shift in potential window during bending may due to change of the surface area of the electrode. However, the device recovery was very fast after bending as shown in Fig. 5(d).

The FSPP has been used as DC source (through a load resistance (R_L) of 5 kΩ) to power continuously a flexible pH sensor. For this purpose, we have used a pH sensor based on nanostructured CuO nanorods, whose fabrication method and characteristics have been thoroughly described elsewhere [36]. To ensure the operation of aforementioned pH sensor, a DC power is supplied across the conducting electrode of the sensor using the FSPP (Fig. 5(e)). Once the FSPP is connected to the pH sensor, we measured the resistance variation of flexible pH sensor based on CuO nanorods (Fig. 5(e)) as a function of different pH solutions. Prior to the pH sensor characterization, the GFSC in the FSPP is fully charged through PV cell under 1 sun illumination (3.8 mW cm^{-2}, $I_{sc} = 26.6$ mA, $V_{oc} = 4.7$ V), using a voltage divider to limit the charging current and voltage up to 0.5 mA and 0.8 V, respectively. In this scenario, the GFSC can supply a potential of 0.8 V to the pH sensor even if we need < 250 mV. Since the power harvested by the PV cell is around 3.8 mW cm^{-2}, the power density of the GFSC is 0.27 mW cm^{-2}, and the power consumption of the pH sensor is in the range of nW cm^{-2}, the connection of the FSPP to the pH sensor guarantees a rapid charging of the GFSC by the PV cell, and a slower discharging than the charging times. These conditions show a continuous operation of a pH sensor without using an external battery (see inset of Fig. 5(f)). This also demonstrates that our GFSC based FSPP is a viable technology for self-powered systems. From that characterization, one can conclude that the output voltage across the sensor is measured as a function of the pH value of the solution under test (Fig. S11 in supplementary). We

have also found that by increasing the pH value of the solution towards basic region the resistance of the pH sensor value increases (Fig. 5f). In an acidic region of the solution, the ions absorbed on the sensitive electrode are mainly hydroxonium ions (H_3O^+), whereas this is done by hydroxyl ions (OH^-) in the basic solution. The slight drift in resistance in pH measurement is due to the lack of stability of pH solution while stirring.

After finishing the measurement, we observed a negligible reduction of GFSC potential of 10 mV, which confirms the rapid charging mechanism carried out by the PV cell alternatively to the slow discharging of the SC from the pH sensor. In good agreement with our previous observations shown in Fig. S12 in Supplementary, we found that the GFSC took around 115 s to drop a voltage of only 15 mV, which make the FSPP suitable to power a pH sensor with a fast response in the range of tens of seconds. From the pH sensing performance, we observed that the pH sensor shows very fast response. The response time of the sensor is less than 5 s from pH 6.38 to pH 4 (from Fig. 5(e)) and from pH 5 to pH 5.8 it is nearly 12 s. This fast response of sensor further highlights the benefits of self-powered system.

With the high energy density and stability of the GFSC based FSPP combined with the low-power consumption of the pH sensor, we have successfully characterized pH sensor with and without sunlight (Fig. 6). The current measured through the SC (I_{SC}) and the pH sensor (I_{pH}) present uniform characteristics with PV cell on (t < 5 min) and off (t > 5 min). Such a platform can be further extended towards a 24 h self-powering systems consisting of multiple nano-/micro-devices, possibly transmitting the data to smartphone, or for applications such as fully-energy-autonomous e-skin for prosthetics and robotics [5].

4. Conclusion

This work presents a novel GFSC with layer-by-layer structure consisting of graphene sheet-Ag-graphene foam as high energy density electrode. Fabricated GFSC exhibited an areal capacitance of 38 mF cm^{-2}, energy density of 3.4 µW h cm^{-2} and power density of
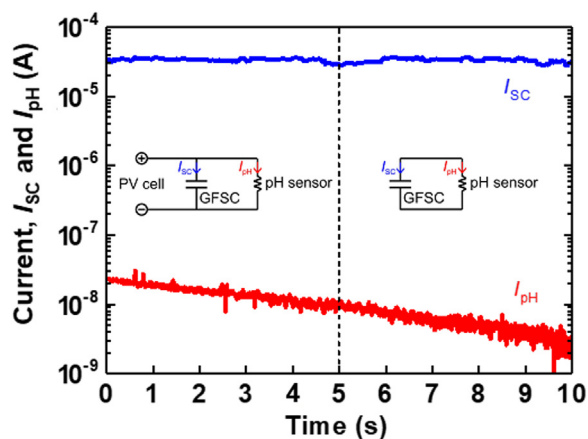
Fig. 6. Current of the pH sensor (I_{pH}) and GFSC (I_{SC}) measured over time using the FSPP with the PV cell on (< 5 min) and off (> 5 min). Inset: equivalent circuits for FSPP.

$0.27\,\text{mW}\,\text{cm}^{-2}$ at current density of $0.67\,\text{mA}\,\text{cm}^{-2}$. The extensive characterization of GFSCs under static and dynamic bending conditions shows that they have excellent electrochemical and supercapacitive performance, which is due to the benefit from Ag conductive epoxy, the high surface area in the porous structure of electrodes and the highly conductivity of free-standing 3D graphene foam. The excellent life cycle of presented GFSCs, with capacitance retention of 68% after 25000 charge/discharge cycles, shows their potential for use in several applications and the suitability for manufacturing. In this regard, GFSC was integrated with a flexible PV cell, resulting in a FSPP capable to produce a continuous DC power. The applicability of the GFSC based FSPP was demonstrated by powering continuously a nanostructured CuO based pH sensor. This technology has demonstrated promising advances towards the successful development of fully self-powered system in areas such as multi-sensing e-skin for robots and human healthcare monitoring.

Appendix A. Supporting information

Supplementary data associated with this article can be found in the online version at doi:10.1016/j.nanoen.2018.06.072.

References

[1] G. Lee, S.-K. Kang, S.M. Won, P. Gutruf, Y.R. Jeong, J. Koo, S.-S. Lee, J.A. Rogers, J.S. Ha, Fully biodegradable microsupercapacitor for power storage in transient electronics, Adv. Energy Mater. 7 (2017) 1700157.
[2] Z. Yuan, X. Du, N. Li, Y. Yin, R. Cao, X. Zhang, S. Zhao, H. Niu, T. Jiang, W. Xu, Z.L. Wang, C. Li, Triboelectric-based transparent secret code, Adv. Sci. (2018) 1700881.
[3] Y. Han, Q. Li, T. Wang, W. Chen, L. Ma, Multisource coordination energy management strategy based on SOC consensus for a PEMFC–battery–supercapacitor hybrid tramway, IEEE Trans. Veh. Technol. 67 (2018) 296–305.
[4] M. Hu, T. Hu, R. Cheng, J. Yang, C. Cui, C. Zhang, X. Wang, MXene-coated silk-derived carbon cloth toward flexible electrode for supercapacitor application, J. Energy Chem. 27 (2018) 161–166.
[5] C. García Núñez, W.T. Navaraj, E.O. Polat, R. Dahiya, Energy-autonomous, flexible, and transparent tactile skin, Adv. Funct. Mater. 27 (2017) 1606287.
[6] J. Bandodkar, J. Wang, Non-invasive wearable electrochemical sensors: a review, Trends Biotechnol. 32 (2014) 363–371.
[7] W. Dang, L. Manjakkal, W.T. Navaraj, L. Lorenzelli, V. Vinciguerra, R. Dahiya, Stretchable wireless system for sweat pH monitoring, Biosens. Bioelectron. 107 (2018) 192–202.
[8] D.P. Dubal, N.R. Chodankar, D.H. Kim, P. Gomez-Romero, Towards flexible solid-state supercapacitors for smart and wearable electronics, Chem. Soc. Rev. 47 (2018) 2065–2129.
[9] B. Song, L. Li, Z. Lin, Z.K. Wu, K.S. Moon, K. S, C.P. Wong, Water-dispersible graphene/polyaniline composites for flexible micro-supercapacitors with high energy densities, Nano Energy 16 (2015) 470–478.
[10] B. Song, K.S. Moon, C.P. Wong, Recent developments in design and fabrication of graphene-based interdigital micro-supercapacitors for miniaturized energy storage devices, IEEE Trans. Compon. Packag. Manuf. Technol. 6 (2016) 1752–1765.
[11] E. Ostfeld, A.C. Arias, Flexible photovoltaic power systems: integration opportunities, challenges and advances, Flex. Print. Electron. 2 (2017) 013001.
[12] J. Jaksik, H.J. Moore, T. Trad, O.I. Okoli, M.J. Uddin, Nanostructured functional materials for advanced three-dimensional (3D) solar cells, Sol. Energy Mater. Sol. Cells 167 (2017) 121–132.
[13] Y.B. Lee, J.K. Han, S. Noothongkaew, S.K. Kim, W. Song, S. Myung, S.S. Lee, J. Lim, S.D. Bu, K.-S. An, Toward arbitrary-direction energy harvesting through flexible piezoelectric nanogenerators using perovskite PbTiO3 nanotube arrays, Adv. Mater. 29 (2017) 1604500.
[14] Z. Lin, J. Chen, X. Li, Z. Zhou, K. Meng, W. Wei, J. Yang, Z.L. Wang, Triboelectric nanogenerator enabled body sensor Network for self-powered human heart-rate monitoring, ACS Nano 11 (2017) 8830–8837.
[15] W.T. Navaraj, S. Gupta, L. Lorenzelli, R. Dahiya, Wafer scale transfer of ultra-thin silicon chips on flexible substrates for high performance bendable systems, Adv. Electron. Mater. (2018) 1700277.
[16] W. Dang, V. Vinciguerra, L. Lorenzelli, R. Dahiya, Printable stretchable interconnects, Flex. Print. Electron. 2 (2017) 013003.
[17] J. Lipomi, B.C.-K. Tee, M. Vosgueritchian, Z. Bao, Stretchable organic solar cells, Adv. Mater. 23 (2011) 1771–1775.
[18] J.A. Rogers, T. Someya, Y. Huang, Materials and mechanics for stretchable electronics, Science 327 (2010) 1603–1607.
[19] A. Nazari, S. Farhad, Heat generation in lithium-ion batteries with different nominal capacities and chemistries, Appl. Therm. Eng. 125 (2017) 1501–1517.
[20] W.T. Navaraj, C. García Núñez, D. Shakthivel, V. Vinciguerra, F. Labeau, D.H. Gregory, R. Dahiya, Nanowire, FET based neural element for robotic tactile sensing skin, Front. Neurosci. 20 (2017) 1–20.
[21] H.S. Yaddanapudi, K. Tian, S. Teng, A. Tiwari, Facile preparation of nickel/carbonized wood nanocomposite for environmentally friendly supercapacitor electrodes, Sci. Rep. 6 (2016) 33659.
[22] M.F. El-Kady, V. Strong, S. Dubin, R.B. Kaner, Laser scribing of high-performance and flexible graphene-based electrochemical capacitors, Science 335 (2012) 1326–1330.
[23] S. Zhang, N. Pan, Supercapacitors performance evaluation, Adv. Energy Mater. 5 (2015) 1401401.
[24] V. Augustyn, P. Simon, B. Dunn, Pseudocapacitive oxide materials for high-rate electrochemical energy storage, Energy Environ. Sci. 7 (2014) 1597–1614.
[25] W. Zuo, R. Li, C. Zhou, Y. Li, J. Xia, J. Liu, Battery-supercapacitor hybrid devices: recent progress and future prospects, Adv. Sci. 4 (2017) 1600539.
[26] Y. Wang, Y. Song, Y. Xia, Electrochemical capacitors: mechanism, materials, systems, characterization and applications, Chem. Soc. Rev. 45 (2016) 5925–5950.
[27] Y. Zhu, S. Murali, M.D. Stoller, K.J. Ganesh, W. Cai, P.J. Ferreira, A. Pirkle, R.M. Wallace, K.A. Cychosz, M. Thommes, D. Su, E.A. Stach, R.S. Ruoff, Carbon-based supercapacitors produced by activation of graphene, Science 332 (2011) 1537–1541.
[28] A. Ramadoss, K.-Y. Yoon, M.-J. Kwak, S.-I. Kim, S.-T. Ryu, J.-H. Jang, Fully flexible, lightweight, high performance all-solid-state supercapacitor based on 3-Dimensional-graphene/graphite-paper, J. Power Sources 337 (2017) 159–165.
[29] J. Liu, L. Zhang, H.B. Wu, J. Lin, Z. Shen, X.W.D. Lou, High-performance flexible asymmetric supercapacitors based on a new graphene foam/carbon nanotube hybrid film, Energy Environ. Sci. 7 (2014) 3709–3719.
[30] L. Zhang, D. DeArmond, N.T. Alvarez, D. Zhao, T. Wang, G. Hou, R. Malik, W.R. Heineman, V. Shanov, Beyond graphene foam, a new form of three-dimensional graphene for supercapacitor electrodes, J. Mater. Chem. A 4 (2016) 1876–1886.
[31] X.-C. Dong, H. Xu, X.-W. Wang, Y.-X. Huang, M.B. Chan-Park, H. Zhang, L.-H. Wang, W. Huang, P. Chen, 3D graphene–cobalt oxide electrode for high-performance supercapacitor and enzymeless glucose detection, ACS Nano 6 (2012) 3206–3213.
[32] Y. Zhao, J. Liu, Y. Hu, H. Cheng, C. Hu, C. Jiang, L. Jiang, A. Cao, L. Qu, Highly compression-tolerant supercapacitor based on polypyrrole-mediated graphene foam electrodes, Adv. Mater. 25 (2013) 591–595.
[33] J. Zhang, J. Wang, J. Yang, Y. Wang, M.B. Chan-Park, Three-dimensional macroporous graphene foam filled with mesoporous polyaniline network for high areal capacitance, ACS Sustain. Chem. Eng. 2 (2014) 2291–2296.
[34] H.B. Yao, J. Ge, C.F. Wang, X. Wang, W. Hu, Z.J. Zheng, Y. Ni, S.H. Yu, A flexible and highly pressure-sensitive graphene–polyurethane sponge based on fractured microstructure design, Adv. Mater. 25 (2013) 6692–6698.
[35] Z. Lou, L. Li, L. Wang, G. Shen, Recent progress of self-powered sensing systems for wearable electronics, Small 13 (2017) 1701791 (13).
[36] L. Manjakkal, S.B. Sakthivel, N. Gopalakrishnan, R. Dahiya, Printed flexible electrochemical pH sensors based on CuO nanorods, Sens. Actuators B-Chem. 263 (2018) 50–58.

[37] J.J. Yoo, K. Balakrishnan, J. Huang, V. Meunier, B.G. Sumpter, A. Srivastava, M. Conway, A.L.M. Reddy, J. Yu, R. Vajtai, P.M. Ajayan, Ultrathin planar graphene supercapacitors, ACS Nano Lett. 11 (2011) 1423–1427.

[38] P. Xu, J. Kang, J.-B. Choi, J. Suhr, J. Yu, F. Li, J.-H. Byun, B.-S. Kim, T.-W. Chou, Laminated ultrathin chemical vapor deposition graphene films based stretchable and transparent high-rate supercapacitor, ACS Nano 8 (2014) 9437–9445.

[39] Q. Chen, X. Li, X. Zang, Y. Cao, Y. He, P. Li, K. Wang, J. Wei, D. Wud, H. Zhu, Effect of different gel electrolytes on graphene-based solid-state supercapacitors, RSC Adv. 4 (2014) 36253–36256.

[40] M. Wu, Y. Li, B. Yao, J. Chen, C. Li, G. Shi, A high-performance current collector-free flexible in-plane micro-supercapacitor based on a highly conductive reduced graphene oxide film, J. Mater. Chem. A 4 (2016) 16213–16218.

[41] D. Pech, M. Brunet, H. Durou, P. Huang, V. Mochalin, Y. Gogotsi, P.-L. Taberna, P. Simon, Ultrahigh-power micrometre-sized supercapacitors based on onion-like carbon, Nat. Nano 5 (2010) 651–654.

[42] J. Zhi, W. Zhao, X. Liu, A. Chen, Z. Liu, F. Huang, Highly conductive ordered mesoporous carbon based electrodes decorated by 3D graphene and 1D silver nanowire for flexible supercapacitor, Adv. Funct. Mater. 24 (2014) 2013–2019.

[43] S. Liu, J. Xie, H. Li, Y. Wang, H.Y. Yang, T. Zhu, S. Zhang, G. Cao, X. Zhao, Nitrogen-doped reduced graphene oxide for high-performance flexible all-solid-state micro-supercapacitors, J. Mater. Chem. A 2 (2014) 18125–18131.

[44] M. Beidaghi, C. Wang, Micro-supercapacitors based on interdigital electrodes of reduced graphene oxide and carbon nanotube composites with ultrahigh power handling performance, Adv. Funct. Mater. 22 (2012) 4501–4510.

[45] Z.-K. Wu, Z. Lin, L. Li, B. Song, K.-s. Moon, S.-L. Bai, C.-P. Wong, Flexible micro-supercapacitor based on in-situ assembled graphene on metal template at room temperature, Nano Energy 10 (2014) 222–228.

[46] Z. Peng, J. Lin, R. Ye, E.L.G. Samuel, J.M. Tour, Flexible and stackable laser-induced graphene supercapacitors, ACS Appl. Mater. Interfaces 7 (2015) 3414–3419.

Carlos García Núñez was born in Segovia, Spain, in 1984. He received his B.S. degree in Physics in 2009, his M.S. degree in Advanced Materials and Nanotechnology in 2010, and his Ph.D. degree in Physics in 2015, in the Department of Applied Physics from Universidad Autónoma de Madrid, Spain. Since 2015, he has been Postdoctoral Researcher with the School of Engineering, University of Glasgow (UK). He is author of 17 journal papers, 9 conference proceedings, 1 book chapter, and 1 patent. His research interest includes synthesis and characterization of semiconductor nanowires for optoelectronics, photovoltaics, electronics and wearable systems.

Wenting Dang received B.Sc. dual degree in electrical and electronics engineering from Nanjing University of Posts and Telecommunications, China and New York Institute of Technology, US in 2011, M.Sc. degree in microsystems engineering from University of Freiburg, Germany in 2013. She started her Ph.D. as a Marie Curie Early Stage Researcher in CONTEST (COllaborative Network for Training in Electronic Skin Technology) project. Currently she is in her last year of Ph.D. study at University of Glasgow, UK. Her work is focused on stretchable interconnects and sensor's integration on conformable and stretchable substrate.

Ravinder Dahiya is Professor of Electronics and Nanoscale Engineering in University of Glasgow. He has published more than 200 articles and has given more than 90 invited talks. He has more than 12 years of experience in the field of flexible electronics and has won several awards including the 2016 IEEE Sensor Council Technical Achievement Award. He is leading the Bendable Electronics and Sensing Technologies (BEST) research group with more than 20 researchers (including 7 post-docs, 12 Ph.Ds).

Libu Manjakkal received B.Sc. and M.Sc degree in physics from Calicut University, and Mahatma Gandhi University, India and Ph.D. degree in electronic engineering from Institute of Electron Technology (ITE), Poland, in 2012–2015 (in a Marie Curie ITN Program). From 2009–2012 he was worked at CMET, India. In 2012, he was with New University of Lisbon, Portugal. From 2015–2016, he was a post-doctoral with ITE. Since 2016, he was a post-doctoral at University of Glasgow, UK. He has authored/co-authored 32 scientific papers. His research interest includes material synthesis, electrochemical sensors, super-capacitors, flexible electronics and wearable systems.